JOURNAL OF AIRCRAFT
Vol. 45, No. 1, January–February 2008

Ground-Based Simulation of Complex Maneuvers of a Delta-Wing Aircraft

Martin Rein* and Gebhard Höhler†
DLR, German Aerospace Center, D 37073 Göttingen, Germany
Andreas Schütte‡
DLR, German Aerospace Center, D 38108 Braunschweig, Germany
and
Andreas Bergmann§ and Thomas Löser¶
DNW, German-Dutch Wind Tunnels, D 38108 Braunschweig, Germany

DOI: 10.2514/1.30033

Ground-based simulations of complex maneuvers of a model of the X-31 aircraft have been performed in the low-speed wind tunnel of the German–Dutch Wind Tunnels. In the wind-tunnel tests a novel test rig with 6 degrees of freedom was used for the first time for moving the model. Furthermore, the model was equipped with eight remotely controlled control surfaces. In this manner, maneuvers in which both the model and its control surfaces were moved simultaneously have been performed. Both the specific technical equipment of the model and the novel 6 degree of freedom test rig will be reviewed. Thereafter, experimental results obtained will be discussed.

Nomenclature

C_D	=	drag coefficient (aerodynamic coordinate system)
C_L	=	lift coefficient (aerodynamic coordinate system)
C_l	=	rolling moment coefficient (aerodynamic coordinate system)
C_m	=	pitching moment coefficient (aerodynamic coordinate system)
C_n	=	yawing moment coefficient (aerodynamic coordinate system)
C_p	=	pressure coefficient
C_y	=	lateral force coefficient (aerodynamic coordinate system)
$\bar{c}$	=	mean aerodynamic chord
f	=	frequency
k	=	reduced frequency, $k = 2\pi f\bar{c}/U_\infty$
leil, leir	=	inner left/right leading edge
leol, leor	=	outer left/right leading edge
rud	=	rudder
T	=	period
t	=	time
tel, ter	=	left/right trailing edge
t_o	=	characteristic time, $t_o = \bar{c}/U_\infty$
U_∞	=	freestream velocity
α	=	angle of attack
β	=	angle of sideslip
η	=	angle of a control surface

Presented as Paper 3149 at the 25th AIAA Aerodynamic Measurement Technology and Ground Testing Conference, San Francisco, CA, 5–8 June 2006; received 26 January 2007; revision received 19 September 2007; accepted for publication 21 September 2007.

*Senior Scientist, Institute of Aerodynamics and Flow Technology, Bunsenstrasse 10; martin.rein@dlr.de (Corresponding Author).
†Research Scientist, Institute of Aerodynamics and Flow Technology, Bunsenstrasse 10.
‡Research Scientist, Institute of Aerodynamics and Flow Technology, Lilienthalplatz 7.
§Director, Low-Speed Wind Tunnel, Lilienthalplatz 7.
¶Research Scientist, Low-Speed Wind Tunnel, Lilienthalplatz 7.

I. Introduction

THE ever increasing maneuverability and agility of modern delta-wing aircraft operating at high angles of attack pose great challenges in the design process. It is well known that already at moderate angles of attack, small changes in the flight conditions can strongly influence the vortex dominated flowfield about the wings and fuselage, and thus result in large changes of the aerodynamic loads. Classical approaches for obtaining dynamic stability information are no longer sufficient. Already in the 1970s a need for improved experimental facilities has been expressed [1]. In the 1990s the reliability of existing capabilities for dynamic wind-tunnel testing, particularly, relating to rotary and oscillatory motions at high angles of attack was explored by an AGARD working group [2]. The comparison of results obtained in different facilities by using the same model geometry shows that results agree well as long as the flow is stable. However, in unstable cases, in particular, if the flow over the forebody is not artificially symmetrized, the specific test conditions become important. Also on the analytical side more and more complex approaches and alternative modeling techniques have been applied [3,4]. Currently, methods based on computational fluid dynamics are becoming realistic tools. In this context a first data base for unsteady aerodynamics including transient motions of fully configured aircraft has been compiled [5]. A step in this direction has also been undertaken for improving design procedures of submarines [6,7]. In an even more advanced multidisciplinary approach presently pursued at DLR, aerodynamical, flight mechanical and structural mechanical aspects are directly coupled [8]. The objective of the present paper is to describe the experimental part in the development of this new tool.

For describing the unsteady aerodynamics of a maneuvering aircraft not only the fluid mechanical equations should be solved but also, simultaneously, the equations of flight mechanics and aeroelastics. This is the topic of a project at DLR where a simulation environment is being developed for coupling a time-accurate flow solver (TAU) with a computational module for solving the flight-mechanics equations of motion and a structural mechanics code for determining structural deformations [8]. The use of an overlapping grid technique allows for treating moving control surfaces as well. This highly challenging approach requires a validation by experimental data. In this context complex maneuvers of a delta-wing aircraft have been simulated in a low-speed wind tunnel thus providing data allowing a validation of the aerodynamics and flight-mechanics coupling. This is the subject of the present paper. As a test object the X-31 aircraft has been chosen because it is an example of a

highly agile aircraft with poststall maneuverability that covers angles of attack up to $\alpha \approx 70$ deg due to thrust vectoring.

To obtain a data base for validating the new numerical simulation tool, ground-based simulations of complex maneuvers of a model of the X-31 aircraft have been performed in the low-speed wind tunnel NWB of the German–Dutch Wind Tunnels DNW. In the wind-tunnel tests a novel test rig with 6 degrees of freedom (DOF) was used for the first time for moving the model. Furthermore, the model was equipped with eight remotely controlled movable control surfaces. In this manner simulations of complete maneuvers of a model with its control surfaces deflecting synchronously with the model's motion were achieved in a ground-based facility. In the following, first, the specific technical equipment of the novel 6-DOF test rig and the model will be reviewed. Thereafter, experimental results obtained will be discussed.

II. Low-Speed Wind Tunnel and Model Positioning Mechanism

During the development of an aircraft it is highly desirable to obtain information about the future handling qualities of the aircraft already at a very early stage. For the experimental determination of the corresponding dynamic derivatives a new combined motion test capability was developed at DNW for its low-speed wind tunnel NWB in Braunschweig, using a 6 DOF test rig called a model positioning mechanism (MPM) as an improved successor to the older systems of mobile oscillatory derivative balance (MOD) and oscillating motion support (OMS) [9]. The test rig (MPM) can be used for oscillating the wind-tunnel model about one body axis through a sinusoidal motion as well as for arbitrary motions about combined axes to simulate flight maneuvers. The first application of the novel MPM was performing wind-tunnel maneuvers with a model of the X-31 aircraft to obtain experimental data for validating a numerical approach of coupling fluid and flight mechanical computations. Besides its application for dynamic tests the MPM is also well suited for static tests in combination with ground effect simulations. In the NWB the MPM is located above the test section. Figure 1 shows a photo of the MPM with a model of the X-31 mounted on a belly sting. Note that the model is mounted upside down.

The major characteristic of the test rig is its high dynamic capability over the whole workspace. In addition, the stiffness has been improved compared with the preceding systems (MOD, OMS). The demands of large amplitude and high-rate arbitrary motions are met by a 6 degree-of-freedom parallel kinematic mechanism resulting in the following advantages compared with a conventional serial axis arrangement:

1) higher dynamics despite identical input power because lower weights are being moved,

2) higher accuracy because errors in parallel kinematics exert less effect,

3) lower costs due to simpler construction and identical components for each axis, and

4) lower demands on tolerances for production and assembly because geometric transformation takes the place of axial alignment.

The main features of the kinematic mechanism are sketched in Fig. 2. The mechanism consists of a movable platform (Stewart platform) which is linked to the wind-tunnel fixed base by six constant length legs that are joined with the platform as well as with six carriages which can move along two parallel guiding rails, so that the position and orientation of the platform can be adjusted. The six carriages run independently of each other on each guiding rail, allowing a displacement within 6 degrees of freedom. Because each guiding rail is shared by three carriages, the design is simplified and has fewer components than previous versions.

The workspace of the MPM spans 1100 mm in the flow direction, 300 mm in the lateral direction, and 500 mm in the heave direction. Because of the parallel kinematics driving the MPM, all parameters, for example, the maximum angles of attack and sideslip and their rates of change, depend on each other and, therefore, a general motion envelope of the MPM cannot easily be defined. Here, in simulating maneuvers, only the rotational degrees of freedom were used. In some cases the range of motion in a particular direction was greatly increased by adding a connecting rod to the MPM (cf. Fig. 3). The connecting rod that is located behind the belly sting drives an additional kinematic mechanism located inside the fuselage. In this

Fig. 1 Model positioning mechanism (MPM) with belly sting and X-31 remote-control model in the low-speed wind tunnel NWB.

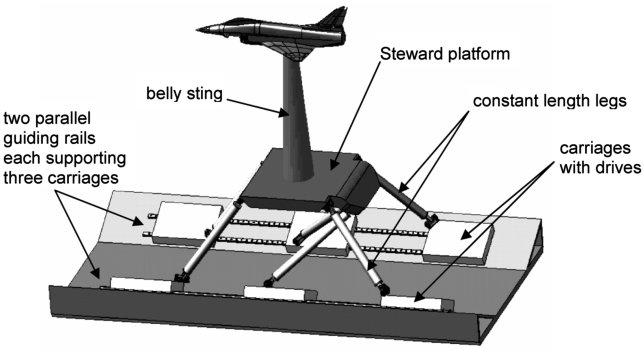

Fig. 2 Sketch of the MPM.

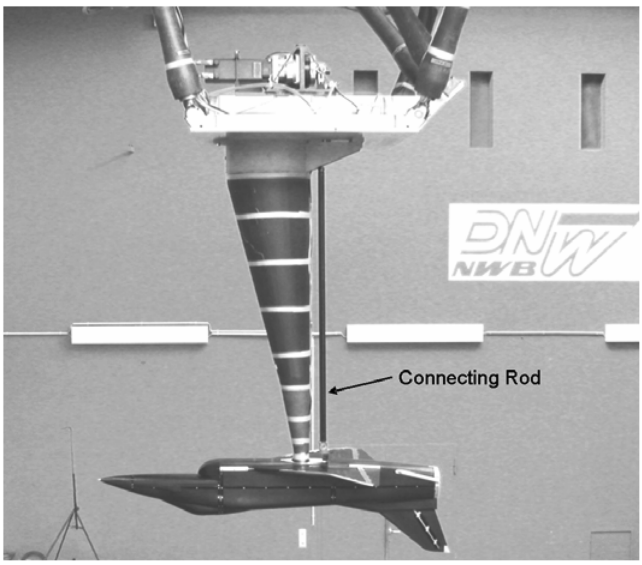

Fig. 3 X-31 lightweight model mounted on belly sting with connecting rod.

manner its transversal motion is transferred into an angular deflection of the model such as roll or pitch, thus enabling a greater range of motion in a particular coordinate. In the present tests the maximum angle of attack was $\alpha = 30$ deg but greater angles could have been achieved by suitably mounting the model. Using the additional kinematic mechanism with connecting rod pitch oscillations with amplitudes up to $\Delta\alpha = 15$ deg were performed at reduced frequencies up to $k = 0.163$, the frequency (and thus acceleration) being limited by the balance used but not by the MPM. The maximum angles of sideslip and roll were $\beta = \pm 10$ deg and $\gamma = \pm 10$ deg, respectively.

For control of the MPM, a numerically controlled milling machine hardware (Sinumerik 840D) in combination with an adapted software is used. To avoid a conventional ballscrew drive with its elasticity in the drive chain the axes are brought into motion by application of the linear direct drive technology. Altogether six Simodrive 1FN3 linear motors are used, allowing accelerations up to 2.5 g. The accuracy of the system in pivoting angles is better than 0.005 deg. At the top of the sting the first eigenfrequency is above 20 Hz. The test rig allows a payload of up to 5000 N. The complex three-dimensional motion of the model is monitored by an optical position tracking system.

The MPM was first used for collecting static data at various angles of attack and sideslip for comparison with reference data. All measurements were performed in the open test section of the $S = 2.85 \times 3.20$ m^2 low-speed atmospheric wind tunnel NWB. With the open test section the maximum flow velocity is 75 m/s and the maximum Reynolds number based on the length $0.1S^{1/2}$ is $Re = 1.8 \times 10^6$. On the axis of the test section the turbulence level is about $Tu = 0.15\%$. In all tests reported in the following the freestream flow velocity was $U_\infty = 60$ m/s. Then the Reynolds number formed with the mean aerodynamic chord ($\bar{c} = 0.518$ m) is $Re \approx 2 \times 10^6$. The X-31 model was mounted to the MPM by a belly sting (cf. Fig. 1). A comparison with static data obtained under otherwise same conditions with the X-31 model mounted on a rear sting always shows good qualitative agreement both in force and moments as well as in wing surface pressure data. Not surprisingly, quantitatively minor differences are present in the pressure data. Because the present measurements are performed to provide validation data for numerical approaches this is of no importance because the belly sting will be included in the calculations anyway. Finally, it should be noted that pressure data obtained on the left and right wings, respectively, agree extremely well (for a zero angle of sideslip) thus showing an excellent symmetry of the model and flow.

III. X-31 Remote-Control Model and Data Acquisition

In the following the specific properties of the model and its instrumentation as well as those of the telemetric system used for transferring the data to an external data acquisition system are outlined.

The X-31 is a single-engine, single-place cockpit, delta-wing aircraft. For control the aircraft has a small canard, a single vertical tail with conventional rudder, wing leading-edge flaps, and trailing-edge flaps. A fully equipped wind-tunnel model of the X-31, the so-called X-31 remote-control model, was developed and built to a scale of about 1:7.25 at the German Aerospace Center DLR (cf. Figs. 1, 3, and 4). The model is made from steel and carbon fiber reinforced plastic. A small nose strake and strakes on the fuselage (cf. Fig. 4) enforce a symmetry of the flow thus providing prerequisites under which results were found to depend little on particular flow conditions in dynamic testing [2]. The control surfaces can be deflected via a remote-control system. The main part of the X-31 model is a wing-fuselage section including eight servomotors for changing the angles η of canard, leading-edge inner and outer flaps, trailing-edge flaps, and rudder (canard: -70 deg $\leq \eta_{\text{canard}} \leq 20$ deg, inner leading-edge flaps: -32 deg $\leq \eta_{\text{lei}} \leq 0$ deg, outer leading-edge flaps: -40 deg $\leq \eta_{\text{leo}} \leq 0$ deg, trailing-edge flaps: -30 deg $\leq \eta_{\text{te}} \leq 30$ deg, rudder: -30 deg $\leq \eta_{\text{rud}} \leq 30$ deg, cf. Fig. 4). The air intake of the model is masked by a cover

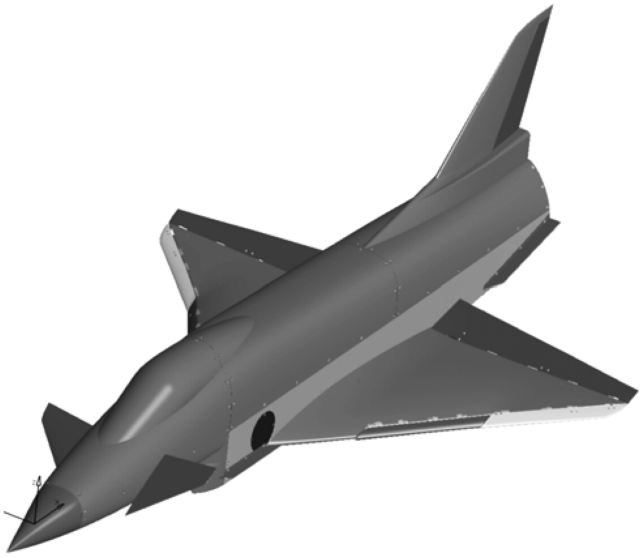

Fig. 4 Sketch of the X-31 remote-control model with strakes, movable canard, inner and outer leading-edge flaps, trailing-edge flaps, and rudder.

(cf. Fig. 3). In addition to the remote-control model whose mass amounts to about 110 kg, a lightweight model has been built to enable motions with higher accelerations.

The models are equipped with pressure and temperature sensors, an inclinometer, and a six component strain gauge balance. At the maximum values of forces and moments obtained in the present tests the accuracy of the corresponding coefficients is 6 and 10% for the normal force and rolling moment coefficient, respectively, and 1 and 5% for the other force and moment coefficients. Unsteady surface pressures are measured by 54 miniature piezoresistive pressure sensors located at two sections on the upper surface of the delta wing and on the leading-edge flaps. Dynamic tests of the pressure sensors performed at absolute pressures ranging from 0.085 to 0.10 MPa have shown that their resolution in time that depends on the way the transducers are assembled into the model is below 1 ms and their accuracy is better than 1% of the stagnation pressure in the wind-tunnel tests. The temperature is measured by two temperature sensors that have been glued to the lower side of the upper wing surface. The static angle of attack is determined by an inclinometer.

All analog signals from the pressure transducers, the balance, inclinometer, and temperature sensors are digitized and amplified by eight electronic modules located in the wing-fuselage section and transferred to the external data acquisition system of DNW-NWB by a 64-channel 16-bit telemetric system. The system also allows for a remote calibration of the pressure transducers. The transfer rate of the telemetric system is about 2.9 kHz so that flow phenomena such as vortex breakdown can be resolved. In the following, data that have been filtered using a low pass filter with a cutoff frequency are presented whenever high frequency phenomena are not the subject of a particular consideration.

IV. Experimental Results and Discussion

To test the capabilities of both the model positioning mechanism and the remote-control model, many different tests were performed. In the following high-amplitude angle of attack oscillations, the influence of flap motions, and a realization of complete maneuvers will be demonstrated. For defining a maneuver the correspondence between the motion of the model and its control surfaces needs to be specified. In the case of complex maneuvers theoretical approaches are not straightforward. Therefore, in the present study wind-tunnel maneuvers have been modeled based on data from real flight tests. In this, the time has been rescaled according to the smaller model size and flow velocity in the wind tunnel. Two maneuvers related to steady-heading sideslip test points and a 2 g pull, respectively, are considered in more detail.

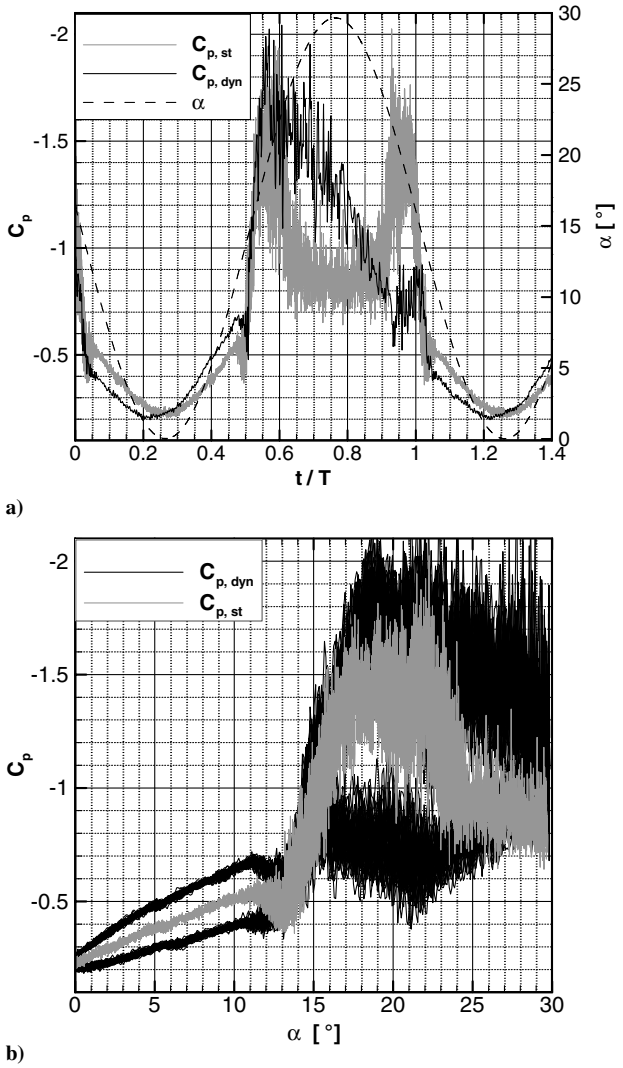

Fig. 5 Quasi-steady and dynamic pitching oscillations of large amplitude ($\alpha_0 = 15$ deg, $\Delta\alpha = 15$ deg; gray lines: $k = 0.005$, black lines: $k = 0.163$), pressure coefficient determined at a representative location on the upper wing surface (cf. text) versus nondimensional time a) and versus angle of attack b). For comparison the variation with the time of the angle of attack is also included in a).

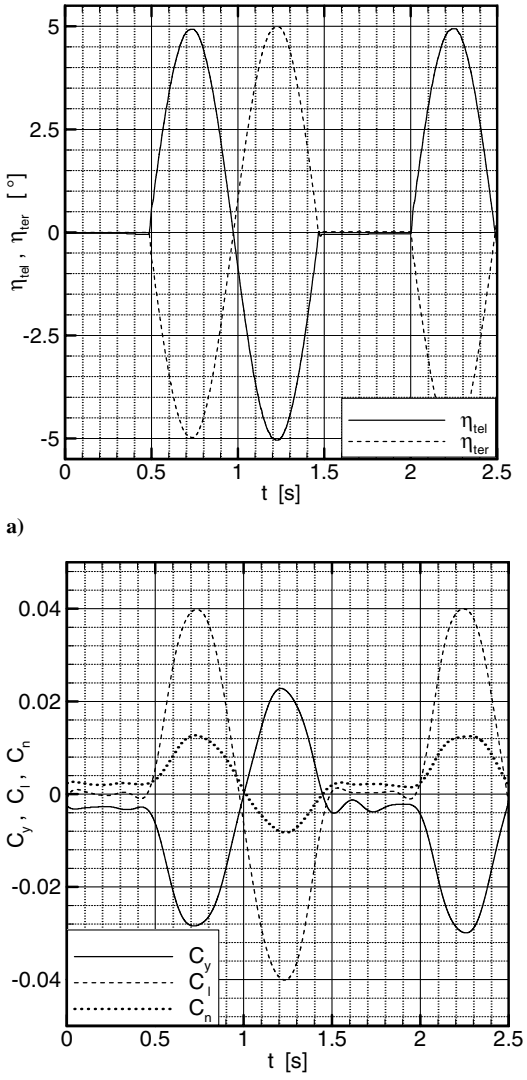

Fig. 6 Sinusoidal motion (antiphase) of trailing-edge flaps for the period of motion corresponding with a reduced frequency of $k = 0.054$: a) variation with time of flap angles (η_{tel}, η_{ter}) and b) of the coefficients of lateral force (C_y), rolling (C_l), and yawing (C_n) moment.

First, let us consider pitching motions of high amplitude. These were enabled by using the connecting rod and attaching it via a pitch module to the model. In this manner amplitudes up to $\Delta\alpha = 15$ deg can be achieved. In all tests with large amplitude pitching oscillations the lightweight version of the X-31 model was used so that high accelerations became possible. As an example an oscillation about $\alpha_0 = 15$ deg with an amplitude of $\Delta\alpha = 15$ deg is considered in Fig. 5. In this case, flows without vortices, with vortices, and with vortex breakdown are encountered during one oscillation cycle. The resulting time dependence of a characteristic pressure coefficient is shown in Fig. 5 for a quasi-steady and an unsteady case. A quasi-steady motion was realized by an oscillation at a small reduced frequeny of $k = 0.005$ ($f = 0.1$ Hz). In the unsteady case also shown in Fig. 5 the reduced frequency is $k = 0.163$ ($f = 3$ Hz). Note that the time is scaled by the oscillation period T. The pressure coefficient shown (C_p) has been determined from unfiltered pressure data obtained at a pressure tap located at the outer part (spanwise direction) on the upper surface of the left wing. At this position the formation and breakdown of vortices can be well detected. In both cases the onset of vortex formation is observed at about the same nondimensional time. However, the dependence on time of the pressure coefficient is clearly unsymmetrical in the dynamic case. This hysteretic behavior is especially well displayed when the pressure coefficient is plotted versus the angle of attack (Fig. 5b). Again, the presence of vortices is recognizable for angles greater than $\alpha \approx 11$ deg in both cases. In the quasi-steady case a decrease in lift caused by vortex breakdown is well recognizable to begin and stop at about $\alpha \approx 22$ deg. In the unsteady case the dynamics cause the well-known opening of the curve [10]. Here, the larger of the two pressure coefficients corresponds always with a decreasing angle of attack. The characteristics of pitching motions performed with frequencies in between the two considered in Fig. 5 smoothly fit into the observed behavior.

In a next step a variety of flap motions was tested with the model remaining in a steady state. Here, the X-31 remote-control model was used. Sinusoidal motions comprising one or two periods were normally executed. In this manner sinusoidal oscillations of the canard, the leading and trailing-edge flaps, and the rudder were performed. Here, the effect of left and right trailing-edge flaps moving in opposing directions, that is, moving in antiphase, will be considered. The flaps are thus acting as ailerons. In the present example the angle of attack is $\alpha \approx 10$ deg. The motion of the two flaps is depicted in Fig. 6a. As can be seen, a single sinusoidal motion with an amplitude of $\Delta\eta_{\text{tel,ter}} = 5$ deg and a period of $T = 1s = 116t_o$, where $t_o = \bar{c}/U_\infty$ is the characteristic time scale, is performed. The motion is repeated after a short time interval. The resulting lateral force coefficient (C_y) is shown in Fig. 6b. Small oscillations occurring at times were the flaps are in a fixed position

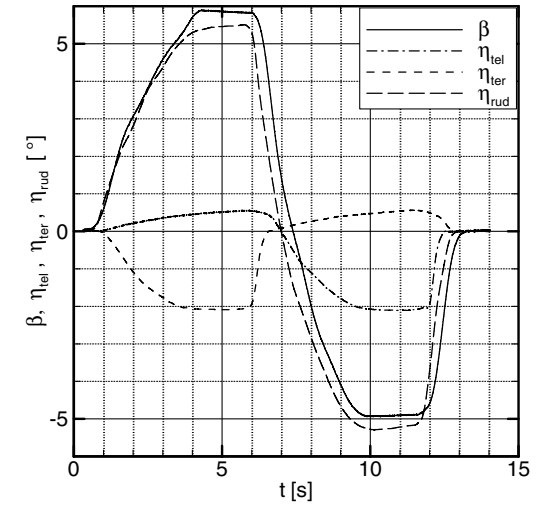

a)

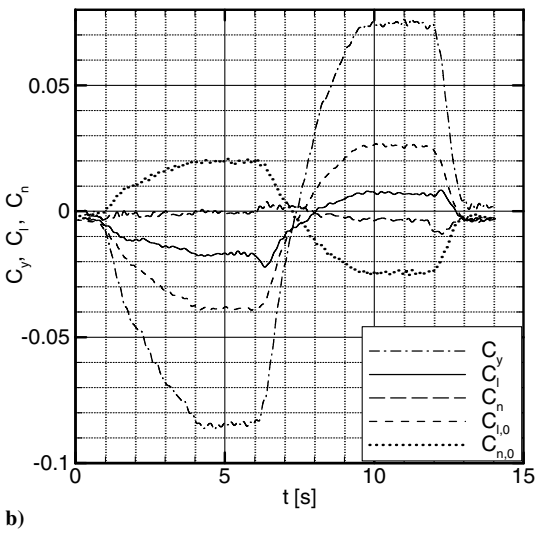

b)

Fig. 7 Simulation of a maneuver (steady-heading sideslip): a) variation with time of sideslip angle β, and angles of control surfaces (η_{rud}, η_{tel}, η_{ter}); b) corresponding coefficients of lateral force (C_y), rolling (C_l), and yawing (C_n) moments. For comparison also the rolling ($C_{l,0}$) and yawing ($C_{n,0}$) moments obtained when all flaps are kept in a zero position are also plotted.

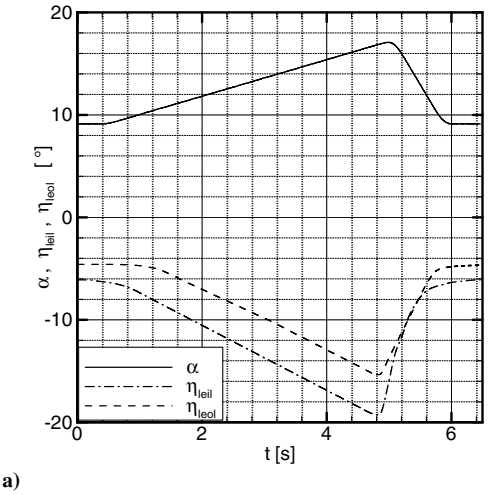

a)

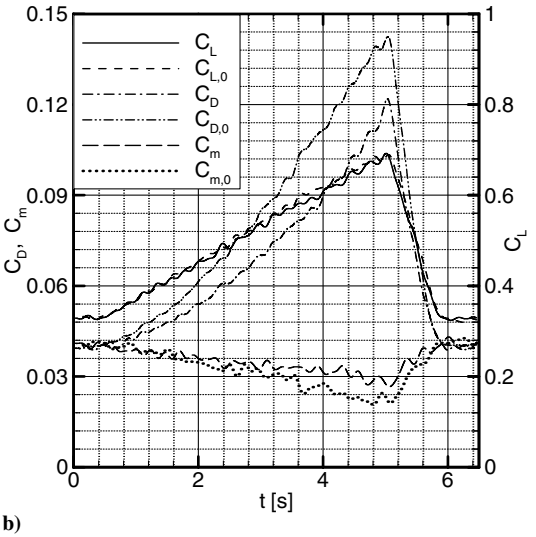

b)

Fig. 8 Simulation of a maneuver (2-*g* pull) with and without (index 0) deflections of the flaps: a) forced dependence on time of the angle of attack and the angles of the leading-edge flaps and b) resulting force and moment coefficients.

are caused by the simple low pass filter applied. The rolling (C_l) and yawing (C_n) moment coefficients corresponding with the lateral force coefficient are also contained in Fig. 6b. These results clearly demonstrate the effect of the remotely controlled flap motions.

The effect of trailing-edge flaps acting as ailerons has been used in performing a wind-tunnel maneuver in which steady-heading sideslip was to be simulated. In this maneuver the rudder performs large motions and the trailing-edge flaps are used to oppose the resulting rolling and yawing moments. The dependence on time of both the angle of sideslip β and all flap angles has again been defined by using data of a real flight maneuver. In this the flight data were smoothed and symmetrized. For example, in the real flight the leading-edge flaps were slightly moving up and down. This motion was not repeated in the wind-tunnel experiment; instead all leading-edge flaps were held at a constant value of $\eta_{\text{le}} = -10$ deg. Similarly, the angle of attack is held at a constant value of $\alpha \approx 11.5$ deg and the canard is aligned in the flow direction, $\eta_{\text{canard}} = -\alpha$, at all times. The dependence on time of the angle of sideslip that was achieved via the MPM and variations of the angles of the rudder and trailing-edge flaps are reproduced in Fig. 7a. Note that the time has been rescaled according to the smaller geometry and flow velocity in the wind-tunnel test. The coefficients of the lateral force and the rolling and yawing moments resulting from this maneuver are shown in Fig. 7b.

As can be seen, the coefficients of the moments remain quite small during the whole maneuver. The yawing motion of the model was repeated with all flaps kept fixed in a zero position. The corresponding results of the rolling ($C_{l,0}$) and yawing moment coefficients ($C_{n,0}$) are included in Fig. 7b. A comparison of the two cases shows that the moments are clearly reduced in the former case thus revealing a strong action of the flap motions.

Another maneuver performed in the wind tunnel was modeled after a so-called 2-*g* pull in flight tests. The time dependence of all angles is again based on smoothed and symmetrized real flight data on a rescaled time. Figure 8a shows the smoothed variations in time of the angle of attack and of the leading-edge flaps of the left wing. In the simulation the variation in time of the canard is adapted to that of the angle of attack so that $\eta_{\text{canard}} = -\alpha$. For symmetry reasons the motion of the leading-edge flaps of the right wing were taken to equal exactly those of the left wing ($\eta_{\text{leir}} = \eta_{\text{leil}}$, $\eta_{\text{leor}} = \eta_{\text{leol}}$), although in the real flight tests the flaps of the right wing performed similar but not the same motions as those of the left wing. This unsymmetrical behavior has likely been caused by unsymmetries of the real X-31 plane that are not present in the models. Finally, small deflections of the trailing-edge flaps are neglected and their angles are set to zero at all times. The coefficients of drag (C_D), lift (C_L), and pitching moment (C_m) measured during the experimental simulation of the maneuver are depicted in Fig. 8b. Although the motion of both the model and its control surfaces was performed very smoothly, the unfiltered data of the balance showed some noise and have been filtered. The wavelength of the undulations on the curves in Fig. 8b

corresponds with the cutoff frequency of the low pass filter applied. To show the effect of the flaps the maneuver was repeated keeping all flaps in a zero position. This results in clearly recognizable differences in the pitching moment coefficient and, particularly, in the drag coefficient which remains much smaller in the former case. Differences in the lift coefficient are quite small. Considering absolute values it is seen that the absolute value of the force vector is only changed by about one-half per cent while its direction is turned by more than one and a half degree. Hence, in this maneuver the leading-edge flaps affect mainly the direction of the force vector.

In the same manner as shown above many more data have been gathered that are to be used for validating the numerical simulation framework that is under development at DLR for calculating a freely flying maneuvering combat aircraft. In the numerical approach a maneuver is realized by a time-accurate coupling of aerodynamics, flight mechanics, and structural mechanics. The results of the present wind-tunnel tests serve to validate the coupling of aerodynamics and flight mechanics.

V. Conclusions

A ground-based method for simulating complex maneuvers has been successfully developed and tested in a subsonic facility using a model of the X-31 aircraft. The MPM, a new test rig with 6 degrees of freedom, was applied for moving the model realizing, for example, high angles of attack as a function of time. Simultaneously, up to eight control surfaces of the X-31 model have been moved according to simulated flight maneuvers. In two examples it was shown that the combined motion of both, the model and its flaps, results in realistic transients of the coefficients of forces and moments. The capability of performing complete maneuvers experimentally in a wind tunnel has thus been demonstrated. This opens the possibility of validating numerical computations in which the integration of the fluid dynamical and flight mechanical equations of motion is directly coupled. This is an important step ahead in the development of a multidisciplinary simulation environment pursued at DLR for predicting unsteady critical states of complex maneuvering aircraft.

The maneuvers simulated as described above were based on data derived from flight tests. However, flight tests and wind-tunnel experiments will always differ in certain aspects. In addition to different orders of magnitude in the Reynolds number, typically details in the geometry such as symmetry properties and engines are not the same. Furthermore, in complex maneuvers the flow velocity may quickly change which cannot easily be modeled in a wind tunnel although small changes could be compensated for by translational motions performed by the MPM. The purpose of the present approach is obtaining data for validating numerical concepts. Therefore it is not necessary to model wind-tunnel maneuvers after real flight maneuvers. An approach to avoid the use of real flight data for defining maneuvers could be performing "real" wind-tunnel maneuvers. Starting from a trimmed state, deflections of a control surface will induce forces and moments that are measured by a balance. Results of real-time flight-mechanics calculations based on these measurements can then be used as an input for the model positioning mechanism for moving the model according to the acting forces and moments. In this manner maneuvers that do not need any input from flight tests can be performed in a wind tunnel.

Acknowledgments

The authors would like to thank H. Haselmeyer and P. Klemens of the German Aerospace Center (DLR) for preparing the new telemetric system and for setting up the control system for moving the control surfaces, and W. Reding of the German–Dutch Wind Tunnels (DNW) for including all newly developed components, that is, the telemetric system, control of flaps, and the MPM, into the data acquisition system of the low-speed wind tunnel, Braunschweig (NWB).

References

[1] Orlik-Rückemann, K. J., "Dynamic Stability Testing of Aircraft—Needs Versus Capabilities," *Progress in Aerospace Sciences*, Vol. 16, No. 4, 1975, pp. 431–447. doi:10.1016/0376-0421(75)90005-6

[2] "Cooperative Programme on Dynamic Wind Tunnel Experiments for Manoeuvring Aircraft," AGARD AR-305, 1996.

[3] Greenwell, D. I., "Frequency Effects on Dynamic Stability Derivatives Obtained from Small-Amplitude Oscillatory Testing," *Journal of Aircraft*, Vol. 35, No. 5, 1998, pp. 776–782.

[4] Pai, T. G., "Wind Tunnel Measurements for Modeling Large Amplitude High Alpha Maneuvers," *Advances in Wind Tunnel Test Techniques*, NAL, Bangalore, India, 2005, pp. 24–34.

[5] "Verification and Validation Data for Computational Unsteady Aerodynamics," RTO TR-26, 2000.

[6] Wetzel, T. G., and Simpson, R. L., "Unsteady Crossflow Separation Location Measurements on a Maneuvering 6:1 Prolate Spheroid," *AIAA Journal*, Vol. 36, No. 11, 1998, pp. 2063–2071.

[7] Rhee, S. H., and Hino, T., "Numerical Simulation of Unsteady Turbulent Flow Around Maneuvering Prolate Spheroid," *AIAA Journal*, Vol. 40, No. 10, 2002, pp. 2017–2026.

[8] Schütte, A., Einarsson, G., Schöning, B., Raichle, A., Alrutz, Th., Mönnich, W., Neumann, J., and Heinecke, J., "Numerical Simulation of Maneuvering Combat Aircraft," *New Results in Numerical and Experimental Fluid Mechanics V*, edited by H.-J. Heinemann, Springer, Berlin, 2006, pp. 103–111.

[9] Bergmann, A., Altenburger, R., and Aul, P., "Bewegungsvorrichtung mit gelenkigen Stäben für eine Plattform mit sechs Freiheitsgraden," Europäische Patentschrift, EP 1 609 563 B1, 2005; see also Bergmann, A., Altenburger, R., and Aul, P., "Movement Device," U.S. Patent Application, US 2006/0254380 A1, 2006.

[10] Nelson, R. C., and Pelletier, A., "The Unsteady Aerodynamics of Slender Wings and Aircraft Undergoing Large Amplitude Maneuvers," *Progress in Aerospace Sciences*, Vol. 39, Nos. 2–3, 2003, pp. 185–248. doi:10.1016/S0376-0421(02)00088-X